Int. J. Heat Mass Transfer. Vol. 28, No. 6, pp. 1173–1186, 1985
Printed in Great Britain

0017-9310/85 $3.00 + 0.00

Laminar natural convection between finitely conducting vertical plates

T. BURCH, T. RHODES and S. ACHARYA
Mechanical Engineering Department, Louisiana State University, Baton Rouge, LA 70803, U.S.A.

(*Received* 22 *May* 1984 *and in final form* 3 *January* 1985)

Abstract—Laminar natural convection between finitely conducting vertical plates has been investigated by a finite-difference procedure. Results are obtained for Grashof numbers of 10, 10^3 and 10^6, wall-to-fluid conductivity ratios of 1 and 10, channel height-to-width ratios of 0.5, 1 and 5 and wall thickness-to-width ratios of 0.1 and 0.5. Results indicate that conduction has a significant influence on the natural convection heat transfer, particularly at high Grashof numbers, low conductivity ratios and high wall thickness-to-channel width ratios. The interface temperature distribution is non-uniform. Both velocity and temperature profiles are significantly influenced by conduction. However, when the velocities are normalized with the inlet velocity, the resulting distributions are remarkably close to the velocity profiles for the constant temperature wall. The total mass flow rates and heat flow rates are observed to increase with Grashof numbers, conductivity ratios and channel height-to-width ratios.

INTRODUCTION

LAMINAR free convection in heated vertical channels is of interest in electronic cooling applications and, has therefore, been studied extensively in the heat transfer literature. Both developing and fully developed flows have been considered. The experimental studies of Elenbaas [1] and the application of the finite-difference method to the boundary-layer equations by Bodoia and Osterle [2] were conducted using symmetric isothermal boundary conditions. Subsequent studies [3, 4] include asymmetric isothermal and isoflux boundary conditions. Numerical studies of laminar free convection in a heated vertical channel have also been performed without using the boundary-layer approximation [5, 6]. Recently, the natural convection in neighboring vertical channels has been studied [7]. However, none of the reported studies have considered the influence of finitely conducting walls on the natural convection heat transfer in a vertical channel. Since finitely conducting walls are a rule rather than an exception, it is important to determine the effect of wall conduction on the convection heat transfer. This effect has been recognized to be significant for external free convection problems [8–10] and it is the intent of this paper to determine the influence of wall conduction on confined or internal free convection.

The geometry of the problem to be considered is shown in Fig. 1. The external vertical surfaces of the channel walls are isothermal while the horizontal boundaries are assumed to be adiabatic. The surface temperature T_h along the external surface of the vertical walls is assumed to be greater than the temperature of the surrounding air T_∞. Since $(T_h - T_\infty) > 0$, a natural convection upflow will be induced between the vertical walls. The thermal conditions along the internal surface of the vertical walls is not known *a priori* to the calculations. Rather, it is an outcome of the coupling of the natural convection between the walls and the two-dimensional conduction in the walls. It is in this regard that the problem considered in this paper is different from the standard problem (with specified thermal conditions along the vertical walls) considered in the literature [1–7].

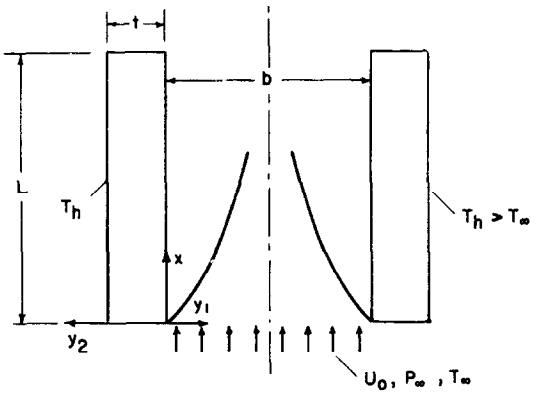

FIG. 1. Vertical channel with conducting walls.

GOVERNING EQUATIONS

The analysis of the physical situation depicted in Fig. 1 must deal with both the energy conservation equation in the wall and the equations of mass, momentum and energy conservation in the fluid. In order to non-dimensionalize the equations, a modified pressure $p' = p - p_\infty$ (where p_∞ is the hydrostatic fluid pressure) is defined and the following dimensionless variables are used

$$X = \frac{x}{L\,Gr}, \quad Y_1 = \frac{y_1}{b}, \quad U = \frac{b^2 u}{Lv\,Gr}, \quad V = \frac{bv}{v} \tag{1}$$

$$P = \frac{p' b^4}{\rho L^2 v^2\,Gr}, \quad \theta = \frac{T - T_\infty}{T_h - T_\infty} \tag{2}$$

NOMENCLATURE

b	channel width
Gr	Grashof number, $g\beta(T_h - T_\infty)b^4/Lv^2$
k_f	fluid thermal conductivity
k_s	solid thermal conductivity
k_r	conductivity ratio, k_s/k_f
L	channel height
$\dot{M}$	dimensionless mass flow rate, equation (10)
Nu	local Nusselt number, hb/k_f
$\overline{Nu}$	average Nusselt number, $\int_0^L Nu\,dx/L$
p	pressure in channel
p_∞	hydrostatic fluid pressure
p'	$p - p_\infty$
P	dimensionless pressure, equation (2)
Pr	Prandtl number
$\dot{q}$	dimensional total heat flow rate
$\dot{q}_i''$	dimensional interface heat flux
$\dot{q}_i''^*(x)$	dimensionless interface heat flux, equation (9)
$\dot{Q}$	dimensionless total heat flow rate, equation (11)
t	wall thickness
T	temperature
T_h	temperature of external vertical surfaces
T_∞	temperature of surroundings
U, V	dimensionless velocities, equation (1)
u, v	velocity components
u_0, U_0	dimensional and dimensionless inlet velocity
X	dimensionless coordinate, $x/L\,Gr$
Y_1	dimensionless coordinate, y_1/b
Y_2'	dimensionless coordinate, $y_2/L\,Gr$
x, y_1, y_2	coordinates.

Greek symbols

β	thermal expansion coefficient
θ	dimensionless temperature, $(T - T_\infty)/(T_h - T_\infty)$
$\theta_i(x)$	dimensionless interface temperature
ν	kinematic viscosity
ρ	density.

where

$$Gr = g\beta(T_h - T_\infty)b^4/Lv^2.$$

The corresponding dimensionless equations become

$$\frac{\partial U}{\partial X} + \frac{\partial V}{\partial Y_1} = 0, \tag{3}$$

$$U\frac{\partial U}{\partial X} + V\frac{\partial U}{\partial Y_1} = \frac{-dP}{dX} + \theta + \frac{\partial^2 U}{\partial Y_1^2}, \tag{4}$$

$$U\frac{\partial \theta}{\partial X} + V\frac{\partial \theta}{\partial Y_1} = \frac{1}{Pr}\frac{\partial^2 \theta}{\partial Y_1^2}. \tag{5}$$

It is important to note that the only parameter remaining in equations (3)–(5) is the Prandtl number Pr which will be assigned the value of 0.7 corresponding to air. The other parameters are either geometrical or arise in the specification of the boundary conditions.

The conservation equations for the fluid are supplemented with velocity and thermal boundary conditions. The thermal and geometric symmetry of the problem implies that only half the channel width need be solved with

$$V = \frac{\partial U}{\partial Y_1} = \frac{\partial \theta}{\partial Y_1} = 0 \tag{6}$$

along the symmetry line. The no-slip velocity boundary condition is imposed at the solid–fluid interface ($Y_1 = 0$). The thermal conditions at the solid–fluid interface [i.e. the local temperature $\theta_i(x)$ and the local heat flux $\dot{q}_i''^*(x)$] are not known beforehand and, as mentioned earlier, are solution-determined outcomes of the calculation procedure. Since the natural convection in the vertical channel is parabolic, velocity and temperature conditions at the channel exit ($X = 1/Gr$) are not required. At the inlet of the channel ($X = 0$), the ambient temperature T_∞ and a uniform inlet velocity U_0 is specified. The pressure P is specified to be zero at both the inlet and exit. It should be noted that only the first derivative of P appears in the equation and therefore, we require only one condition for P. The additional condition on P is used to replace the missing velocity information at the inlet. The correct choice of U_0 will satisfy the $P = 0$ condition at the exit. Thus, U_0 is iteratively adjusted until $P = 0$ at $X = 1/Gr$.

The equation governing conduction in the wall is the two-dimensional, steady-state heat conduction equation. Assuming constant thermal conductivity in the wall and introducing the same dimensionless variables as for the convection case, this equation is given as

$$\frac{k_r}{Pr}\left(\frac{\partial^2 \theta}{\partial X^2} + \frac{L^2\,Gr^2}{b^2}\frac{\partial^2 \theta}{\partial Y_2^2}\right) = 0 \tag{7}$$

where $Y_2 = y_2/b$ is measured from the solid–fluid interface and directed away from the symmetry line. Equation (7) can be recast in a more convenient form by introducing $Y_2' = Y_2 b/L\,Gr$. Equation (7) then transforms to

$$\frac{k_r}{Pr}\left(\frac{\partial^2 \theta}{\partial X^2} + \frac{\partial^2 \theta}{\partial Y_2'^2}\right) = 0. \tag{8}$$

The boundary conditions along the external vertical surfaces are $\theta = 1$, while along the horizontal walls $\partial\theta/\partial X$ is equal to zero. At each point along the solid–fluid interface, the heat transferred to the surface by conduction must be equal to the heat transferred from

the surface by convection. Thus,

$$\left[\frac{k_r}{Pr}\frac{\partial\theta}{\partial Y'_2}\right]_{Y'_2=0} = -\frac{L\,Gr}{b}\left[\frac{1}{Pr}\frac{\partial\theta}{\partial Y_1}\right]_{Y_1=0}. \quad (9)$$

In addition, the temperature must be continuous at each point along the solid–fluid interface.

SOLUTION METHODOLOGY

As noted earlier, the temperature and the heat flux at the solid–fluid interface $\theta_i(x)$ and $\dot{q}''^*_i(x)$ are not known beforehand and must be determined from the solution. However, the solution of the natural convection equations and the heat conduction equation require the specification of $\theta_i(x)$ and $\dot{q}''^*_i(x)$. Thus, an iterative solution scheme is necessary to obtain the final solution.

The solution methodology encompasses two levels of iteration. The primary iterative loop involves alternately solving the conduction and convection portions with each program using current boundary information supplied by the other. A secondary level of iterations is performed at each visitation to the convection problem and is required in order to correctly specify the inlet velocity.

The procedure is initiated by specifying a tentative temperature profile $\theta_i(x)$ at the solid–fluid interface. Usually the converged temperature profile from a previous case is used. The natural convection problem is then solved based on the assumed temperature boundary condition. The heat flux distribution $\dot{q}''^*_i(x)$ obtained from this solution is then used as an input to the wall conduction equation. The solution of the conduction equation yields a new interface temperature profile $\theta_i(x)$.

To begin the next cycle of iteration, the new values of $\theta_i(x)$ are imposed as boundary conditions for the natural convection problem, the solution to which yields new values of boundary heat flux $\dot{q}''^*_i(x)$ which are then used as the boundary conditions for the conduction equation. This procedure of alternate visitation is repeated until convergence is attained. To determine if the solutions have converged, the change in the dimensionless local temperature in each cycle of calculation is determined and when the maximum change is less than 0.5%, convergence is deemed to have been attained. This convergence criteria typically produces a maximum change of the local heat flux of less than 0.05% in one cycle of calculation. Typically between nine and 12 iterations are required to obtain satisfactory convergence. Due to the strong interaction between the conduction and convection problems, under-relaxation of the interface temperatures $\theta_i(x)$ is helpful in obtaining converged solutions.

The natural convection solutions at each visitation are obtained using a Patankar–Spalding type finite-difference procedure [11]. This implicit finite-difference scheme is a marching method which begins at the channel inlet ($X = 0$) and proceeds step by step until the channel exit ($X = 1/Gr$) is reached. As noted previously this method requires that the velocity U be specified at the channel inlet $X = 0$. Since U_0 is unknown it must be assigned a tentative value to start the computations (usually the inlet velocity from the corresponding isothermal interface solution is a satisfactory guess; for subsequent visitations, the velocity from the previous visitation is used as the starting guess). If the computed pressure at the channel exit is not equal to zero, the inlet velocity is adjusted and the boundary-layer solution in the channel is again obtained. If, once again, the pressure at the exit is not zero, the inlet velocity is re-adjusted by linearly extrapolating (or interpolating) to $P(X = 1/Gr) = 0$ from the U_0 and $P(X = 1/Gr)$ values of the two solutions obtained so far. This extrapolated (or interpolated) inlet velocity is used to obtain the solution again and this velocity U_0 and the exit pressure P are used in combination with the previous two trials to quadratically extrapolate (or interpolate) to $P\,(X = 1/Gr) = 0$. The value of U_0 produced by this quadratic procedure almost invariably produces an exit pressure that falls within the convergence criteria requiring the pressure at the exit to be less than 0.05% of the maximum absolute value of P that exists anywhere in the channel.

The boundary-layer calculations are performed with 100 cross-stream grid points and 5500 forward steps. The deployments of the grid points are carefully tailored to provide grid independent results. The cross-stream grid points are concentrated near the wall where larger gradients are expected to be present. Also, the forward step size is much smaller near the channel inlet and is gradually increased in the flow direction. The accuracy of the numerical procedure is verified by obtaining solutions for the constant wall temperature case (i.e. no wall conduction) and comparing the results with those of other authors. This comparison for the dimensionless mass flow rate $\dot{M}$ and the total heat transfer rate $\dot{Q}$ is shown in Table 1. For each Grashof value considered, the present results are found to be within the range of previously published data.

Attention will now be focused on the solution of the wall heat conduction equation. This equation is solved using a control volume based, finite-difference procedure. Results are obtained using 190 control volumes along the length of the wall ($X = 0$ to $X = 1/Gr$) and 40 control volumes across the width of the wall ($Y'_2 = 0$ to $Y'_2 = t/L\,Gr$). Once again, the grid points are concentrated near $X = 0$ due to the high heat fluxes expected in this region.

Since fewer grid points in the X-direction are needed for the conduction program than in the convection program, each conduction control volume at the solid–fluid interface contains typically 10 or more forward steps of the convection marching procedure. This non-alignment of the two sets of grid points is taken into account in the transfer of boundary information between the two solutions. For the conduction solution the heat flux at the solid–fluid interface is taken to be the distance-weighted average of the fluxes computed in the adjoining boundary-layer forward steps. For the

Table 1. Comparison of the mass flow rates $\dot{M}$ and total heat transfer rate $\dot{Q}$ between different authors for constant temperature walls

Author	$Gr = 10$, $L/b = 0.5$		$Gr = 10^3$, $L/b = 0.5$	
	$\dot{M}$	$\dot{Q}$	$\dot{M}$	$\dot{Q}$
Elenbaas [1]	—	0.207	—	2.214
Bodia and Osterle [2]	0.325	0.199	—	2.493
Aung *et al.* [3]	0.382	0.191	9.60	2.571
Present authors	0.382	0.191	9.34	2.459

boundary-layer solution the solid–fluid interface temperature is correctly incremented each time the marching procedure encounters a new conduction control volume. To avoid interpolation in passing boundary information, the forward step size in the convection program is adjusted so that each conduction control volume boundary is exactly aligned with a forward step location in the natural convection calculation.

RESULTS AND DISCUSSION

The governing parameters in the present problem are the Prandtl number Pr, the Grashof number Gr, the channel height to width ratio L/b, the ratio of wall thickness to channel width t/b and the ratio of the thermal conductivity of the wall to the fluid thermal conductivity k_r. Results are obtained for Grashof numbers of 10, 10^3 and 10^6, L/b values of 0.5, 1 and 5, t/b values of 0.1 and 0.5 and conductivity ratios of 1, 10 and 100. In presenting the results, the solutions for the isothermal wall case (i.e. no wall conduction) are used as a basis for comparison. The dimensionless temperature and heat flux profiles along the solid–fluid interface are of particular interest and are presented first. This is followed by cross-sectional temperature and velocity profiles at selected x/L locations along the channel. Finally, the total mass flow rates and total heat transfer rates are presented in a tabular form.

Interface temperatures

Figures 2–4 present the temperature distribution along the solid–fluid interface (θ_i) for Grashof numbers of 10, 10^3 and 10^6 respectively. The lower part of each figure shows the influence of the t/b parameter while the upper portion highlights the effect of the channel height-to-width ratio L/b. In general, the minimum value for θ_i is at $x/L = 0$ and increases in the streamwise direction. This is only to be expected, since near the inlet the thermal boundary-layer thickness is small and the temperature of the fluid washing the interface is low. This results in high heat fluxes and depressed temperatures. As the thermal boundary layer grows, the temperature of the fluid increases and is associated with lower interface fluxes and higher interface temperatures.

Attention should first be focussed on the lower plots in Figs. 2–4. It may be observed that for each Grashof number, decreasing k_r or increasing t/b tends to lower the interface temperature θ_i. This behavior is easily understood, since the thermal resistance of the wall increases with decreasing k_r and increasing t/b, resulting in a larger temperature drop across the wall and therefore smaller interface temperatures. The influence of wall conduction appears to become increasingly more pronounced with increasing Grashof number. For example, at $Gr = 10^6$ and $L/b = 0.5$, average interface temperatures as low as 0.1 are obtained (at $t/b = 0.5$ and $k_r = 1.0$). Furthermore, the conduction in the walls is clearly two-dimensional in view of the non-uniform interface temperature distribution.

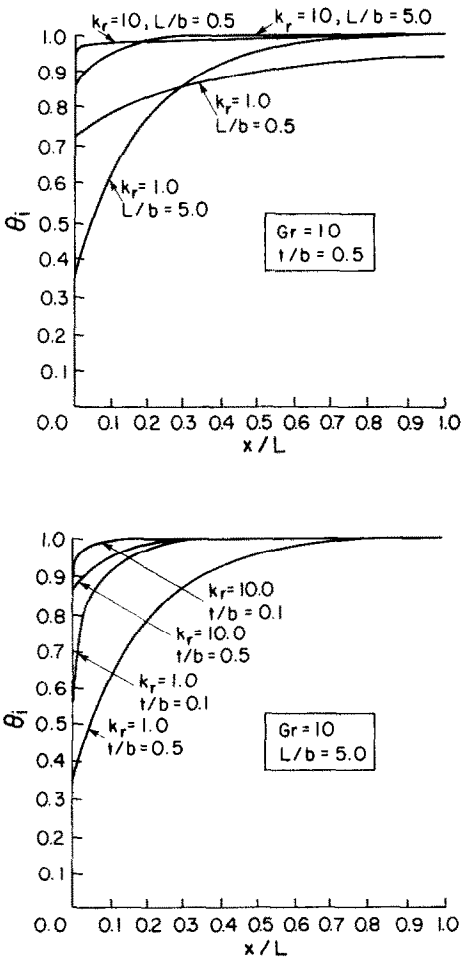

FIG. 2. Interface temperature profiles for $Gr = 10$.

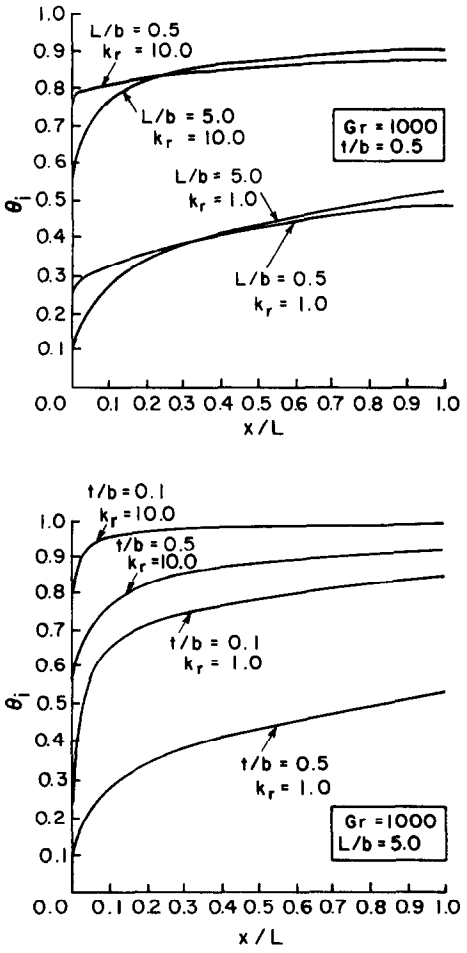

FIG. 3. Interface temperature profiles for $Gr = 10^3$.

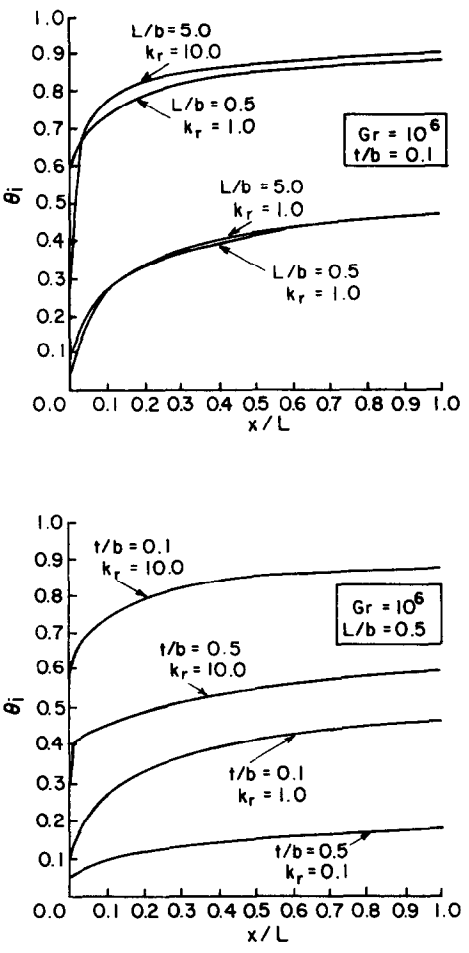

FIG. 4. Interface temperature profiles for $Gr = 10^6$.

The upper plots in Figs. 2–4 indicate that as the length-to-width ratio of the channel is increased, the temperature profiles become more non-uniform. In other words, as L/b is increased from 0.5 to 5, the θ_i values become smaller near the channel inlet and larger near the exit. To explain this behavior, it should be noted that by increasing L/b the heat transfer area (at a fixed inter-plate spacing) increases and therefore, the heat flow rate to the fluid is increased. This, in turn, increases the inlet flow velocity. Higher flow velocities imply a smaller thermal boundary layer at inlet and therefore higher heat fluxes and lower interface temperatures. Furthermore, the faster flow is associated with a higher heat transfer coefficient which explains the steeper slope (near the inlet) of the θ_i curve at a larger L/b value.

The interface temperature distribution at $Gr = 10$, 10^3 and 10^6 are presented in Fig. 5 for $t/b = 0.5$ and $L/b = 0.5$. As mentioned earlier, higher Grashof numbers are associated with lower values for θ_i. This behavior is linked to the higher flow velocities at the larger Grashof numbers which are responsible for higher heat transfer coefficients at the interface and therefore, lower interface temperatures. Furthermore, the influence of the conductivity ratio k_r is less significant at $Gr = 10$ than at 10^3 or 10^6.

Interface heat fluxes

The Local Nusselt number Nu or the dimensionless heat flux $\dot{q}_i''^*$ at the solid–fluid interface is defined as

$$\dot{q}_i''^* = Nu/Pr = (b/Pr)\dot{q}_i''/k_f(T_h - T_\infty)$$
$$= -[(\partial\theta/\partial Y_1)/Pr]_{Y_1=0}. \quad (10)$$

The $\dot{q}_i''^*$ distributions are presented in Figs. 6–8 for Grashof numbers of 10, 10^3 and 10^6. The heat flux distribution for the constant temperature wall channel is also shown in each figure (by short dashed lines). It should be pointed out that the L/b parameter does not explicitly appear in the natural convection equations and therefore, the $\dot{q}_i''^*$ distribution for the constant wall temperature is the same at all L/b.

As expected, the heat flux distribution decreases monotonically from a high value at the channel inlet, with the decrease being particularly rapid near the inlet and more gradual near the exit. The heat flux distribution at $Gr = 10^3$ and 10^6 are shown in Figs. 7 and 8. Since, for the constant wall temperature channel,

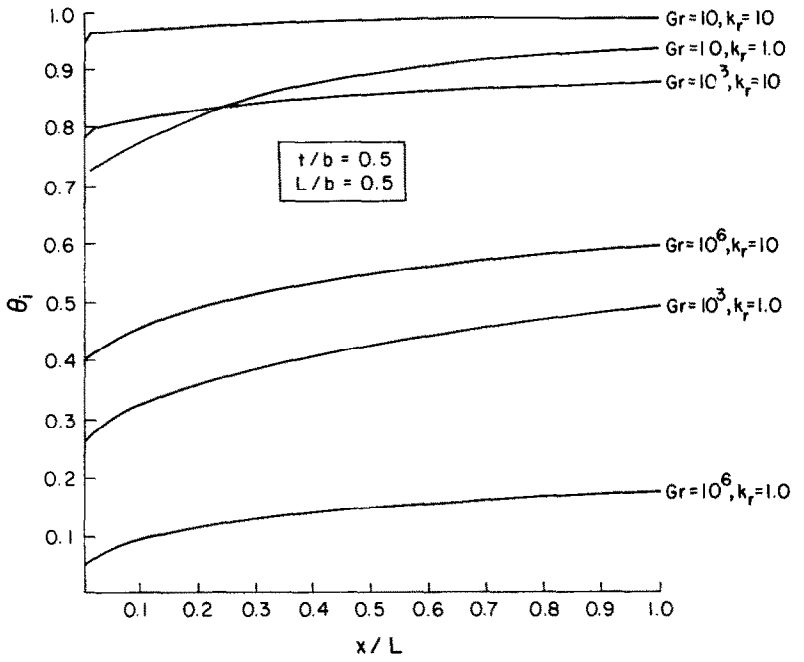

FIG. 5. Interface temperature profiles for $Gr = 10, 10^3, 10^6$.

the temperature difference between the wall and incoming fluid is larger than the corresponding temperature difference for the conducting wall channel, the heat flux values for the constant temperature channel are higher. The difference between the constant wall temperature curves and the conducting wall curves is the smallest for high k_r and low t/b values. This is because increasing k_r and decreasing t/b values result in θ_i values that are closer to 1 (the dimensionless value for the constant wall temperature case). Also, as in the interface temperature profiles, the interface heat flux curves exhibit a steeper slope near the channel inlet at a higher L/b value. Again, this behavior is attributable to the higher heat flow rates at larger L/b values which, in turn, are responsible for higher flow velocities and inlet heat transfer coefficients.

In Fig. 8, the $\dot{q}_i''^*$ distributions for natural convection along a hot vertical plate [12] are also presented. The heat flux values are lower than the corresponding values for the constant wall temperature channel. This is not unexpected since the velocity at the boundary layer edge in the vertical channel is non-zero while the corresponding velocity for the vertical plate is zero. The heat flux distribution at the higher k_r value is expectedly (since θ_i values are higher) closer to the heat flux distribution for the vertical plate.

The trends for the heat flux distribution at $Gr = 10$ (Fig. 6) are somewhat unexpected and different than those observed at $Gr = 10^3$ (Fig. 7) and 10^6 (Fig. 8). It is observed that in the neighborhood of the channel inlet, the heat flux values for the constant wall temperature channel are higher than the corresponding values for the conducting walls. However, beyond a certain x/L value (in the range 0.1–0.2) this trend reverses with the heat flux values for the constant wall temperature becoming smaller than the corresponding conducting wall values. Similarly, the $\dot{q}_i''^*$ curves for $k_r = 1$ lie below the corresponding curve for $k_r = 10$ near the channel inlet but lie above the $k_r = 10$ curve for x/L greater than a value in the range of 0.1–0.2. Also, the heat flux values are smaller near the channel inlet for $t/b = 0.5$ than for $t/b = 0.1$. As before, this trend reverses for x/L values beyond the range of 0.1–0.2.

The higher heat flux values near the channel inlet for the constant wall temperature case is in keeping with the expected trends observed at $Gr = 10^3$ and 10^6. Similarly, the higher fluxes near the channel inlet obtained at higher k_r values and lower t/b values are expected in view of the corresponding higher interface temperatures and inlet flow velocities. However, higher heat fluxes near the inlet implies more energy input into the buoyant flow which, in turn, results in a more rapid increase in the streamwise fluid temperature and therefore, a more rapid decrease of the interface heat flux. It is because of this that the observed cross-over in the flux distribution at $Gr = 10$ is obtained. At higher Grashof numbers this cross-over is not obtained and is due to the increased influence of wall conduction which yields significantly smaller interface temperatures.

The heat flux distribution for different Gr values is plotted in Fig. 9. Expectedly, at a higher Grashof number, the heat flow rates are larger in view of the faster flow velocities. For $Gr = 10$ and $k_r = 10$, the heat flux distribution for the constant temperature wall is nearly indistinguishable from the corresponding curve for the conducting wall. However, the influence of wall conduction and the difference between the two curves increases with increasing Gr and decreasing k_r.

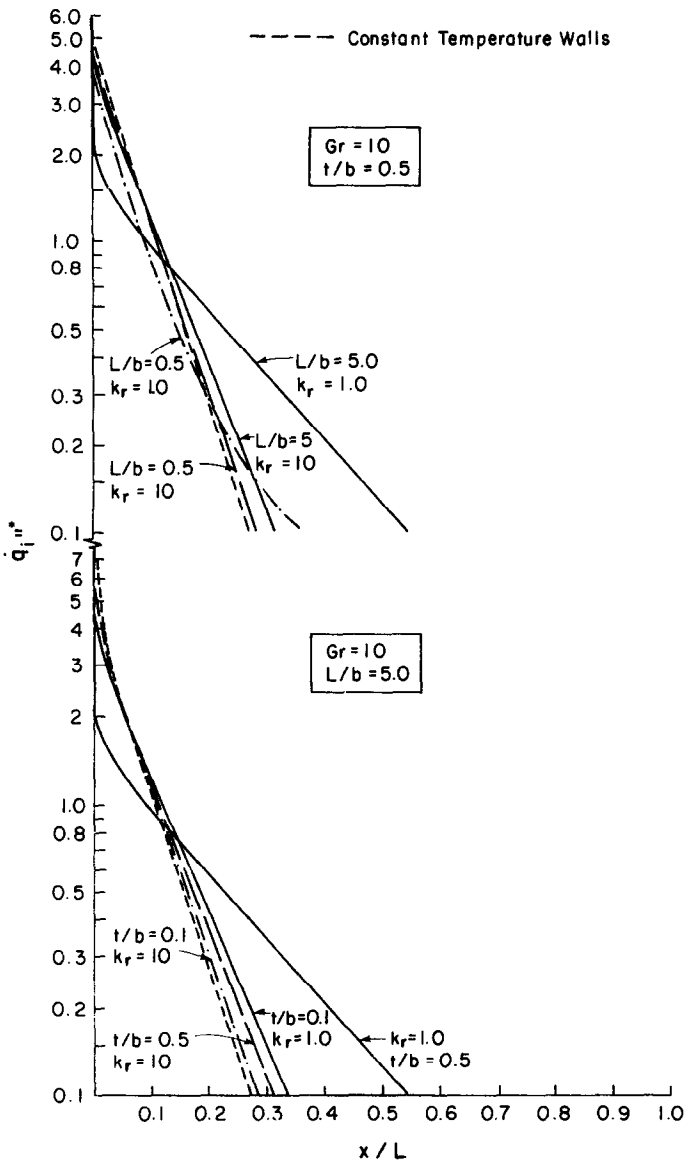

FIG. 6. Interface heat flux profiles for $Gr = 10$.

Temperature and velocity profiles

The temperature profiles in the wall and in the natural convection boundary layer will be presented next. Figure 10 shows the temperature distribution at $Gr = 10$ and $k_r = 1.0$. Significant differences (10–30%) in the natural convection temperature profile arise when the influence of conducting walls is accounted for. The influence of t/b is shown in Fig. 10 and, at any x/L location, the temperature deviation from the constant temperature wall values are expectedly larger at $t/b = 0.5$ than at $t/b = 0.1$. At $Gr = 10$, the differences in the temperature profiles are clearly evident near the channel inlet but diminish at sufficiently large x/L values. If the Grashof number is increased from 10 to 10^6 [Fig. 11(b)] the temperature drop across the wall increases significantly (by as much as a factor of 8 near the channel inlet) due to the higher flow velocities and, therefore, interface heat transfer coefficients.

The influence of the k_r and L/b parameters on the temperature profile at $Gr = 10^6$ is demonstrated in Fig. 11. Increasing k_r from 1 [Fig. 11(b)] to 10 [Fig. 11(a)] expectedly shifts the temperature profile of the conducting wall closer to the constant wall temperature distribution. However, the temperature profile is considerably less sensitive to changes in L/b. When L/b is increased from 0.5 [Fig. 11(b)] to 5 [Fig. 11(c)] the temperature profiles are only slightly altered.

The velocity profile at different (x/L) locations is plotted in Fig. 12 for $Gr = 10, L/b = 5, t/b = 0.5$ and $k_r = 1$ and in Fig. 13 for $Gr = 10^6$, $L/b = 0.5$, $t/b = 0.5$ and $k_r = 1$. Profiles for the dimensionless velocity, as defined in equation (1), are keyed to the vertical axis on

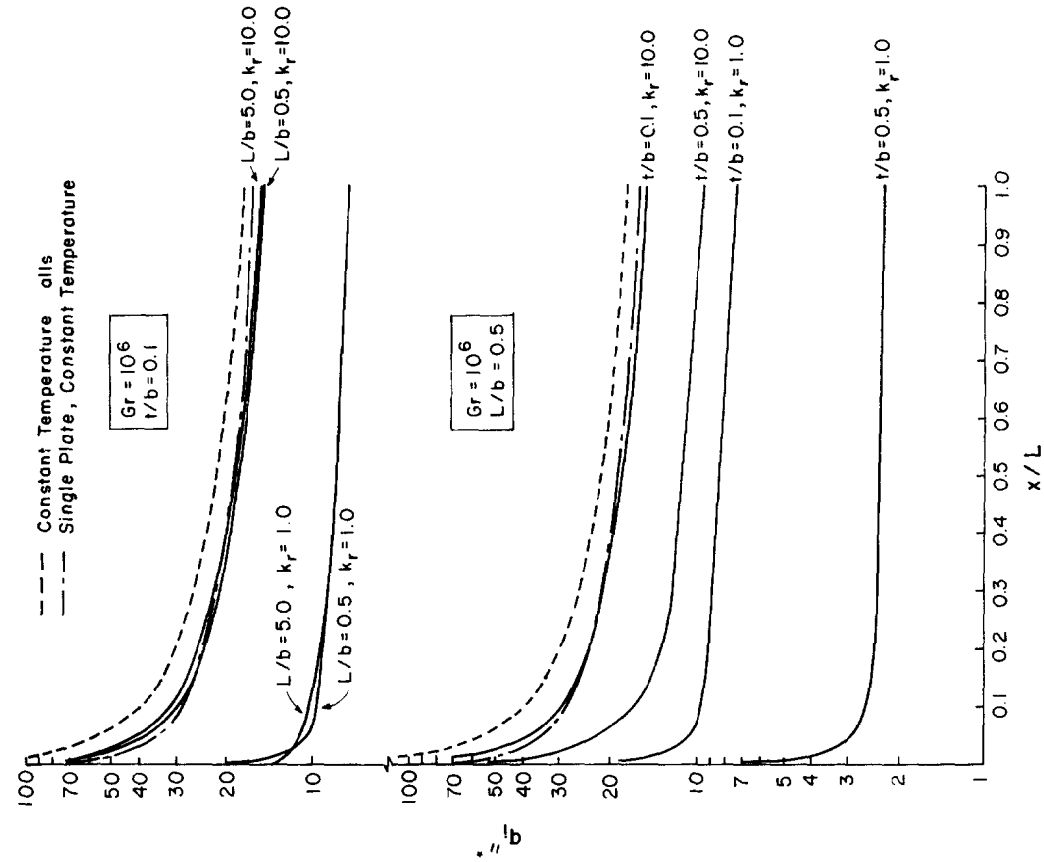

FIG. 8. Interface heat flux profiles for $Gr = 10^6$.

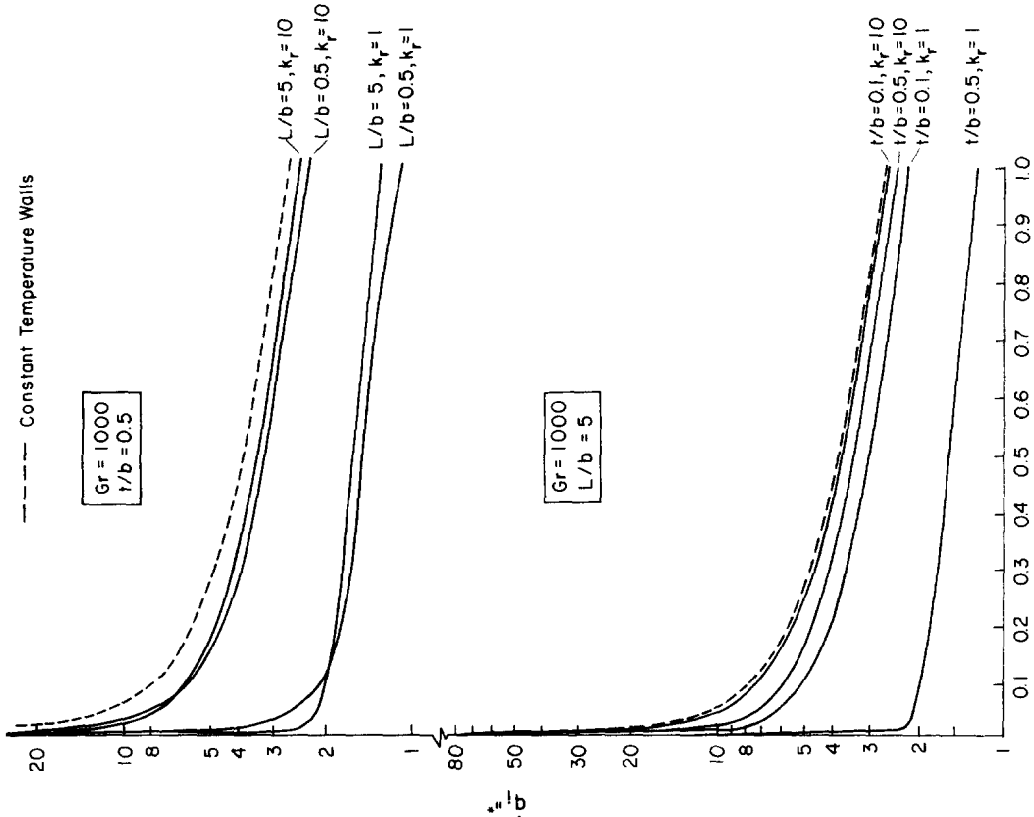

FIG. 7. Interface heat flux profiles for $Gr = 10^3$.

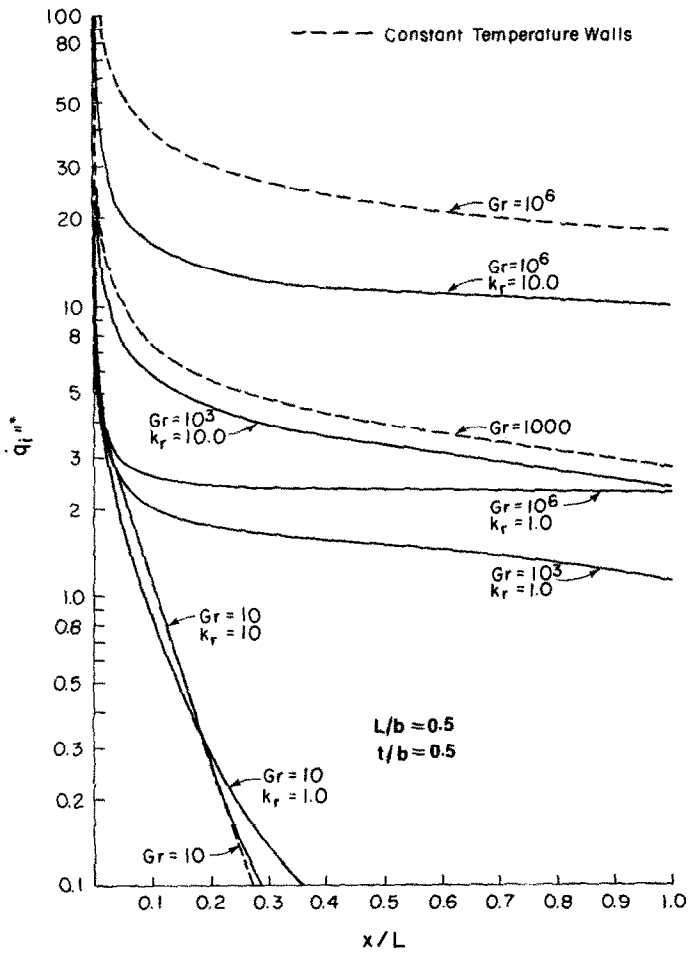

FIG. 9. Interface heat flux profiles for $Gr = 10, 10^3, 10^6$.

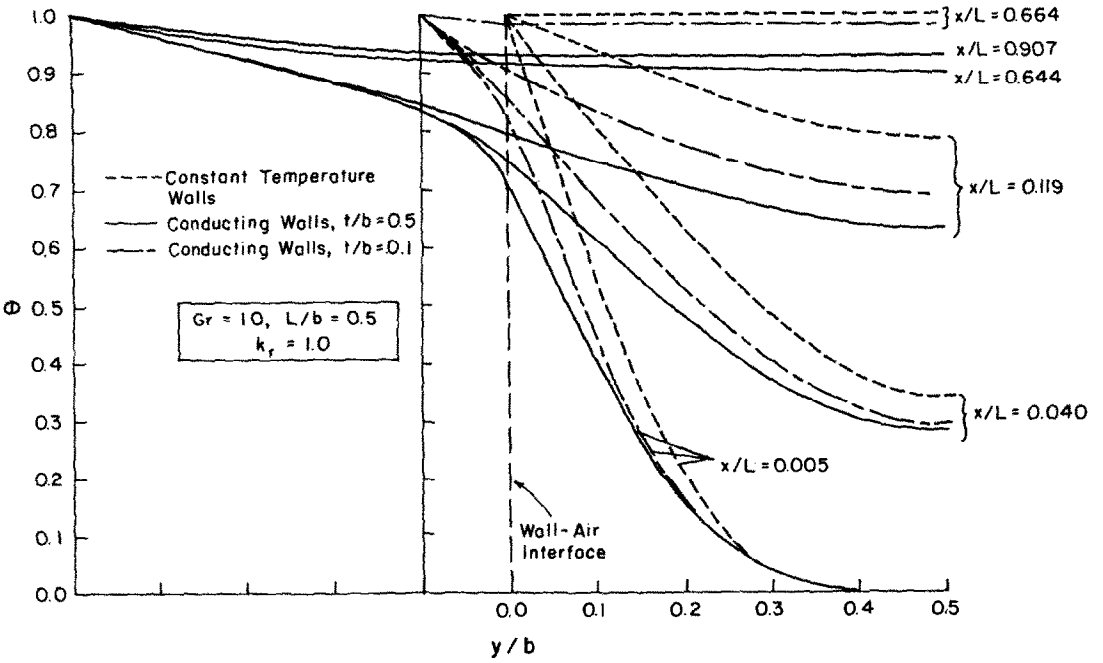

FIG. 10. Temperature profiles at different x/L locations for $Gr = 10$.

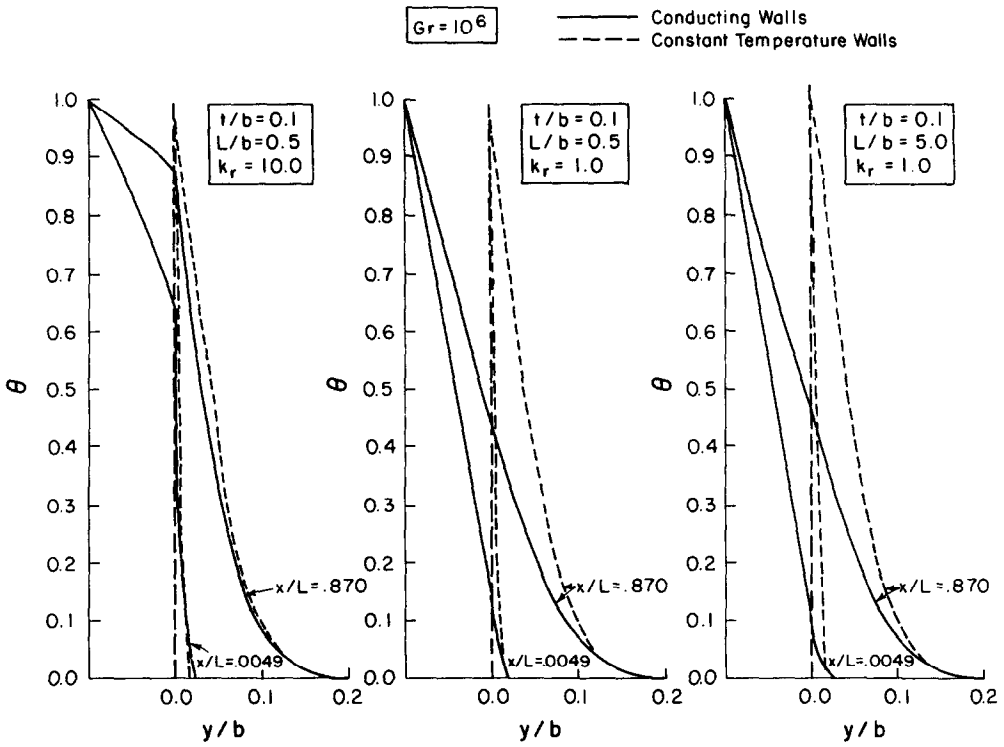

FIG. 11. Temperature profiles at different x/L locations for $Gr = 10^6$.

the right and the horizontal axis on the top. Also plotted, are the velocity profiles made dimensionless with the inlet channel velocity. These curves correspond to the vertical axis on the left and the horizontal axis at the bottom of the plot.

The dimensionless velocity [equation (1)] profiles show that for $Gr = 10$ (Fig. 12) the velocity in the presence of wall conduction is lower (by 10–15%) than the corresponding constant wall temperature case (shown by dotted lines). The velocity profiles develop quite rapidly as evidenced by the very small change in the velocity profile from $x/L = 0.04$ to $x/L = 0.907$.

When the velocity is scaled by the inlet velocity, the discrepancy between the velocity profiles for the conducting wall channel and those of the constant temperature wall channel become much smaller [with only a 1–2% difference in the profile near the channel centerline as compared to the differences of the order of 15% obtained in the velocity profiles which are non-dimensionalized according to equation (1)]. The weaker influence of conduction on the U/U_0 profile (compared to its influence on the U profile) is observed over the complete range of parameter values corresponding to $Gr = 10$.

Similar trends in the velocity profiles are observed at $Gr = 10^6$ although, the differences in the profiles (between the constant temperature channel and the conducting wall channel) are significantly larger. The dimensionless velocities for the conducting wall channel are nearly a third of the velocity values for the constant temperature wall. When normalized with respect to the mean inlet velocity, the discrepancy between the curves is again significantly reduced to a value in the range of 1–15%.

To explain the trends in Figs. 12 and 13 it should be noted that since the interface temperatures in a conducting wall channel are smaller than the constant temperature wall channel value of 1, the entrained flow in the channel is correspondingly slower. Thus, since both U and U_0 are reduced when conduction in the channel wall is accounted for, the ratio U/U_0 is considerably less sensitive to the influence of wall conduction than the individual values of U and U_0.

Axial pressure distribution

The dimensionless axial pressure $-(p-p_\infty)/\rho(v/b)^2$ is plotted in Fig. 14 for $Gr = 10$ and 10^6. As expected, the pressure p decreases from the inlet to a minimum followed by a pressure recovery. The initial pressure drop is proportional to the inlet flow velocity while the pressure recovery is due to buoyancy forces which, in turn, is determined by the interface heat flux $\dot{q}_i''$. For $Gr = 10^6$, the inlet velocity and the interface heat flux is highest for the constant wall temperature channel and decreases with decreasing k_r (Fig. 8). Therefore, the magnitude of pressure drop and recovery is largest for the constant wall temperature channel and decreases with decreasing conductivity ratio for the conducting channel (Fig. 14). For $Gr = 10$, this trend is reversed; in other words, the pressure drop and recovery is smallest for the constant wall temperature channel and increases with decreasing conductivity ratio for the

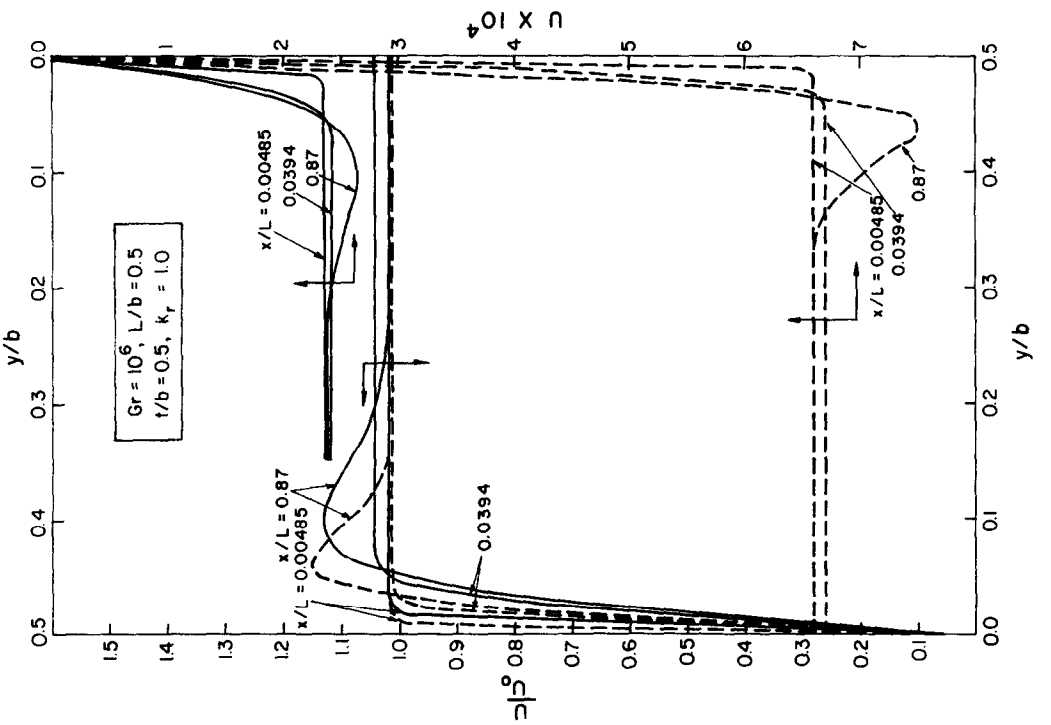

FIG. 13. Velocity profiles at different x/L locations for $Gr = 10^6$.

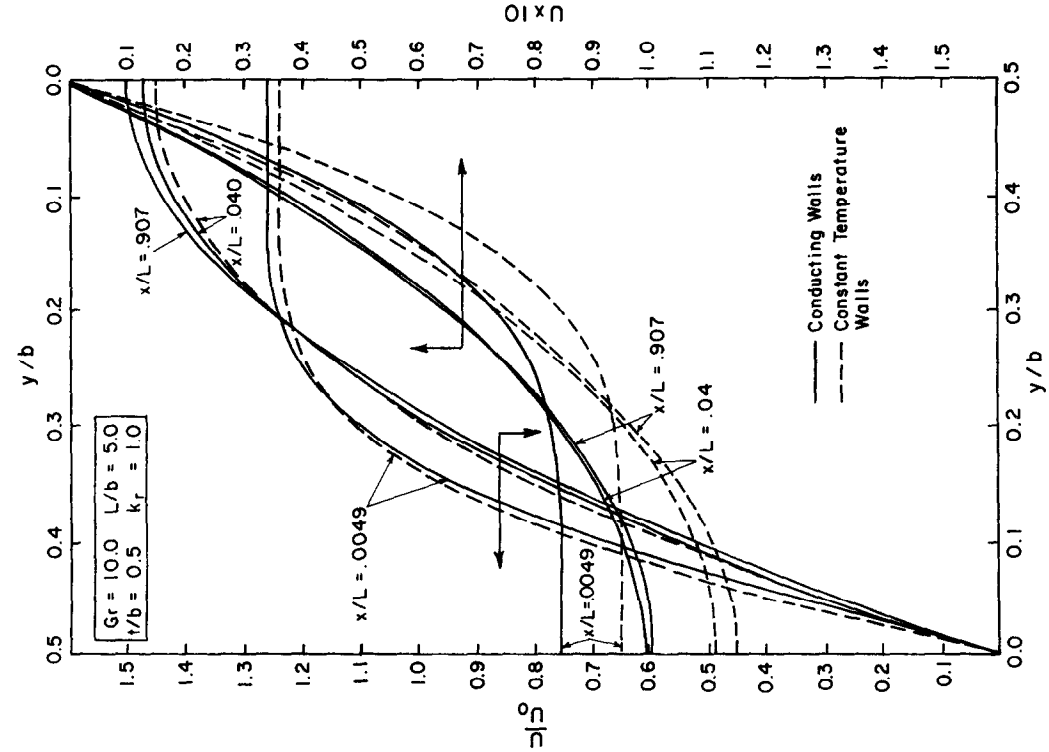

FIG. 12. Velocity profiles at different x/L locations for $Gr = 10$.

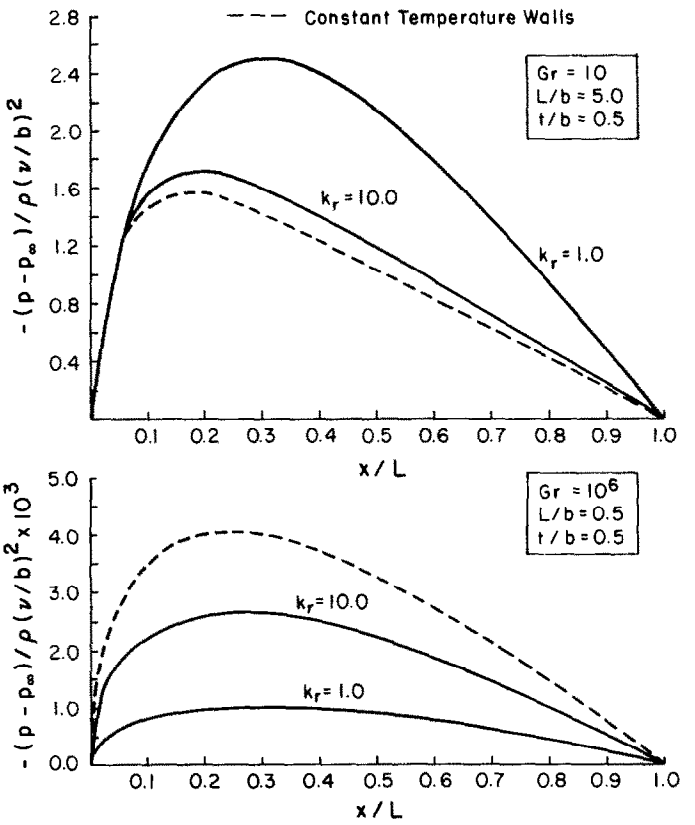

FIG. 14. Dimensionless axial pressure for $Gr = 10, 10^6$.

conduction channel. To explain this, the relative insensitivity of the mass flow rate (i.e. inlet velocity) to k_r should be noted for $Gr = 10$ from Table 3. However, Fig. 6 indicates that the interface heat flux along most of the channel is smallest for the constant wall temperature channel and increases with decreasing k_r. It is because of this that the pressure drop and recovery is smallest for the constant wall temperature channel and increases with decreasing k_r.

Mass flow rates and total heat transfer rate

The dimensionless mass flow rate in the channel $\dot{M}$ and the dimensionless total heat flow rate $\dot{Q}$ from the channel wall to the fluid (or the average Nusselt number $\overline{Nu}$) are defined by the following equations,

$$\dot{M} = u_0 b/\nu = Gr\,(L/b)\int_0^1 U\,\mathrm{d}Y_1 \qquad (11)$$

$$\dot{Q} = \overline{Nu}\,(L/b) = \dot{q}/\{k_f\,Pr\,(T_h - T_\infty)\}$$

$$= Gr\,(L/b)\int_0^{1/Gr} (-1/Pr)(\partial\theta/\partial Y_1)_{Y_1=0}\,\mathrm{d}X \qquad (12)$$

where $\dot{q}$ is the dimensional total heat flow rate from the channel wall.

In Tables 2 and 3, the computed values for $\dot{M}$ and $\dot{Q}$ are tabulated for selected parameter values. Table 2

Table 2. Mass flow rates and total heat flow rates at $Gr = 10^3$

L/b	t/b	k_r	$\dot{M}$	$\dot{Q}$
	Constant wall temperature		9.3375	2.459
		0.1	7.795	1.746
	0.01	1.0	9.130	2.359
		10.0	9.315	2.449
0.5		1.0	7.790	1.737
	0.1	10.0	9.115	2.349
		100.0	9.265	2.419
		1.0	5.505	0.817
	0.5	10.0	8.505	2.022
		100.0	9.240	2.406
	Constant wall temperature		18.675	4.918
		1.0	15.330	3.338
1.0	0.1	10.0	18.260	4.716
		100.0	18.630	4.894
		1.0	10.850	1.642
	0.5	10.0	16.920	4.048
	Constant wall temperature		93.375	24.588
		1.0	77.950	17.459
5.0	0.1	10.0	91.250	23.586
		100.0	93.150	24.481
		1.0	54.100	8.310
	0.5	10.0	84.400	20.350

Table 3. Mass flow rates and heat flow rates at $Gr = 10, 10^6$

Gr	L/b	t/b	k_r	$\dot{M}$	$\dot{Q}$
10	0.5	Constant wall temperature		0.382	0.191
		0.1	1.0	0.368	0.182
		0.1	10.0	0.381	0.190
		0.5	1.0	0.338	0.158
		0.5	10.0	0.377	0.187
	5.0	Constant wall temperature		3.823	1.912
		0.1	1.0	3.717	1.858
		0.1	10.0	3.811	1.905
		0.5	1.0	3.354	1.670
		0.5	10.0	3.767	1.884
10^6	0.5	Constant wall temperature		326.55	13.839
		0.1	1.0	195.25	4.344
		0.1	10.0	293.25	10.953
		0.5	1.0	116.35	1.221
		0.5	10.0	234.56	6.429
	5.0	Constant wall temperature		3256.50	138.386
		0.1	1.0	1955.50	43.616
		0.1	10.0	2955.00	112.213
		0.5	10.0	2322.95	65.352

corresponds to $Gr = 10^3$ and includes a longer list of parameter values, some of which (viz. $t/b = 0.01$, $k_r = 0.1$ and 100) have not been discussed so far. Table 3 lists the $\dot{M}$ and $\dot{Q}$ values at a $Gr = 10$ and 10^6.

From Table 2, it may be observed that increasing k_r leads to higher $\dot{Q}$ and $\dot{M}$ values. This is due to the smaller temperature drop across the walls which is responsible for higher interface temperatures and temperature gradients. Expectedly, a similar behavior is observed with decreasing values of t/b. Also, at a higher L/b value, the heat input $\dot{Q}$ into the fluid is larger which in turn, is responsible for an increase in the mass flow rate. In general, it is observed that at a $k_r = 10$, the heat flow rates are within 20% and the mass flow rates within 10% of the constant temperature case. At a lower k_r however, the percentage differences are considerably more. For example, at $k_r = 1.0$ and $t/b = 0.5$ the $\dot{Q}$ values are nearly 65% lower and the $\dot{M}$ values nearly 40% smaller than the corresponding constant temperature channel values.

As the Grashof number is increased from 10 to 10^6, the buoyancy effects are strengthened and lead to higher inlet velocities and mass flow rates. Higher velocities are associated with higher interface heat fluxes resulting in larger overall heat transfer rates. This trend of increasing $\dot{M}$ and $\dot{Q}$ values with increasing Grashof numbers is evident by a comparison of Tables 2 and 3. Also, the stronger influence of wall conduction at higher Grashof numbers can be noted by comparing the $\dot{M}$ and $\dot{Q}$ values listed in Tables 2 and 3. For example, with $L/b = 0.5, t/b = 0.5$ and $k_r \geq 1$, the $\dot{Q}$ and $\dot{M}$ values at $Gr = 10$ are each approximately 12% lower when the channel walls are conducting as compared to the corresponding values for the constant temperature wall channel. At $Gr = 10^3$, the decrease in $\dot{Q}$ and $\dot{M}$ is about 67% and 41%, respectively while at $Gr = 10^6$ the $\dot{Q}$ values are reduced by as much as 91% and the $\dot{M}$ values by 65%.

CONCLUDING REMARKS

The influence of wall conduction on the natural convection heat transfer between finitely conducting vertical walls is found to be significant, particularly at higher Grashof numbers and lower conductivity ratios. The interface temperatures θ_i and heat fluxes $q_i''^*$ are observed to be non-uniform, with θ_i increasing and $q_i''^*$ decreasing from the channel inlet to the exit. In general, the θ_i values decrease with increasing Gr and t/b, and with decreasing k_r values. For $Gr = 10^3$ and 10^6, the interface heat flux distribution for the constant temperature channel forms the upper bound for the flux distribution obtained for the conducting wall channel. However, at $Gr = 10$, the curves (of interface heat flux) for constant wall temperature channel and the curves for the conducting wall channel cross each other near $x/L = 0.2$. Like the interface temperature distribution, the heat flux distributions are more strongly influenced by wall conduction at a higher Grashof number. The velocity and temperature profiles at different streamwise locations are significantly influenced by wall conduction. However, when the velocity profiles are normalized with the inlet velocity, the profiles for the conducting wall and the constant temperature channel are remarkably close to each other. The mass flow rates and the heat flow rates are observed to increase with increasing Grashof numbers, increasing conductivity and length-to-width ratios, and decreasing wall thickness ratios.

REFERENCES

1. W. Elenbass, Heat dissipation of parallel plates by free convection, *Physica* **9**, 1–28 (1942).
2. J. R. Bodoia and J. F. Osterle, The development of free convection between heated vertical plates, *J. Heat Transfer* **84**, 40–44 (1962).
3. W. Aung, L. S. Fletcher and V. Sernas, Developing laminar free convection between vertical flat plates with asymmetric heating, *Int. J. Heat Mass Transfer* **15**, 2293–2308 (1972).
4. W. Aung, Fully developed laminar free convection between vertical plates heated asymmetrically, *Int. J. Heat Mass Transfer* **15**, 577–1580 (1972).
5. C. F. Kettleborough, Transient laminar free convection between heated vertical plates including entrance effects, *Int. J. Heat Mass Transfer* **15**, 883–896 (1972).
6. H. Nakamura, Y. Asako and T. Naitou, Heat transfer by free convection between two parallel flat plates, *Num. Heat Transfer* **5**, 95–106 (1982).
7. E. M. Sparrow and W. Q. Tao, Buoyancy-driven fluid flow and heat transfer in a pair of interacting vertical parallel channels, *Num. Heat Transfer* **5**, 39–58 (1982).
8. E. M. Sparrow and S. Acharya, A natural convection fin with a solution-determined nonmonotonically varying

heat transfer coefficient, *J. Heat Transfer* **103,** 218–225 (1981).
9. M. Miyamoto, J. Sumikawa, T. Akiyoshi and T. Nakamura, Effects of axial heat conduction in a vertical flat plate on free convection heat transfer, *Int. J. Heat Mass Transfer* **23,** 1545–1553 (1980).
10. K. Kishinami and N. Seki, Natural convective heat transfer on an unheated vertical plate attached to an upstream isothermal plate, *J. Heat Transfer* **105,** 759–766 (1983).
11. S. V. Patankar and D. B. Spalding, *Heat and Mass Transfer in Boundary Layers*. Intertext, London (1970).
12. W. M. Kays and M. E. Crawford, *Convective Heat and Mass Transfer*. McGraw-Hill, New York (1980).

CONVECTION NATURELLE LAMINAIRE ENTRE DES PLAQUES VERTICALES ET CONDUCTRICES

Résumé—La convection naturelle laminaire entre des plaques verticales et conductrices est étudiée par une procédure aux différences finies. Des résultats sont obtenus pour des nombres de Grashof de 10, 10^3 et 10^6, des rapports de conductivité de la paroi au fluide de 1 et 10, des hauteurs de canal rapportées à la largeur égale à 0,5, 1 et 5 et des rapports épaisseur de paroi/largeur de 0,1 et 0,5. Les résultats montrent que la conduction a une influence significative sur la convection naturelle et le transfert thermique, particulièrement aux grands nombres de Grashof, aux faibles rapports de conductivités et aux grandes épaisseurs de paroi. La température sur l'interface n'est pas uniforme. Les profils de vitesse et de température sont influencés par la conduction. Néanmoins quand les vitesses sont normalisées par rapport à la vitesse d'entrée, les distributions résultantes sont remarquablement proches des profils de vitesse à température de paroi constante. Le débit-masse total et le flux de chaleur global sont croissants avec le nombre de Grashof, le rapport des conductivités et le rapport de la hauteur du canal à la largeur.

LAMINARE NATÜRLICHE KONVEKTION ZWISCHEN VERTIKALEN PLATTEN VON ENDLICHER LEITFÄHIGKEIT

Zusammenfassung—Die laminare natürliche Konvektion zwischen vertikalen Platten von endlicher Leitfähigkeit wurde mit einem Finite-Differenzen-Verfahren berechnet. Es liegen Ergebnisse für Grashof-Zahlen von 10, 10^3, 10^6, für das Verhältnis der Wärmeleitfähigkeiten von Wand und Fluid von 1 und 10, für die Verhältnisse von Spalthöhe zu Spaltweite von 0,5, 1 und 5 und für die Verhältnisse Wanddicke zu Spaltweite von 0,1 und 0,5 vor. Die Ergebnisse zeigen den bedeutenden Einfluß der Wärmeleitung auf den Wärmeübergang bei natürlicher Konvektion, besonders bei großen Grashof-Zahlen, bei kleinen Verhältnissen der Wärmeleitfähigkeiten und großen Verhältnissen Wanddicke zu Spaltweite. Die Temperaturverteilung an der Grenzfläche ist nicht gleichförmig. Sowohl das Geschwindigkeits- als auch das Temperaturprofil wird stark durch die Wärmeleitung beeinflußt. Solange die Geschwindigkeiten auf die Eintrittsgeschwindigkeit normiert werden, sind diese Verteilungen ähnlich den Geschwindigkeitsprofilen für konstante Wandtemperatur. Es wurde beobachtet, daß die Gesamtmassenströme und die Wärmeströme mit der Grashof-Zahl, dem Wärmeleitverhältnis und dem Verhältnis Spalthöhe zu Spaltweite ansteigen.

ЛАМИНАРНАЯ ЕСТЕСТВЕННАЯ КОНВЕКЦИЯ МЕЖДУ ВЕРТИКАЛЬНЫМИ ПЛАСТИНАМИ КОНЕЧНОЙ ТЕПЛОПРОВОДНОСТИ

Аннотация—Методом конечных разностей исследована ламинарная естественная конвекция между вертикальными пластинами с конечной теплопроводностью. Получены результаты для чисел Грасгофа 10, 10^3 и 10^6, отношений теплопроводностей стенки и жидкости 1 и 10, отношений высоты к ширине канала 0,5; 1 и 5 и толщины стенки к ширине 0,1 и 0,5. Эти результаты показывают, что теплопроводность существенно влияет на естественноконвективный теплоперенос особенно при больших числах Грасгофа, малых отношениях теплопроводностей и больших отношениях толщины стенки к ширине канала. Распределение температуры на границе является неравномерным. На профили скорости и температуры сильно влияет теплопроводность. Однако, при нормировании скоростей по скорости на входе получающиеся распределения заметно приближаются к профилям скорости для стенки с постоянной температурой. Замечено, что скорости полных потоков массы и скорости теплообмена возрастают с увеличением чисел Грасгофа, соотношений теплопроводностей и отношений высоты канала к его ширине.